Dual Fluorescence and Intramolecular Charge Transfer with *N*-Phenylphenanthridinones

Attila Demeter* and Tibor Bérces

Institute of Chemistry, Chemical Research Center, Hungarian Academy of Sciences, 1025 Budapest, Pusztaszeri u. 59-67, Hungary

Klaas A. Zachariasse

Max-Planck-Institut für biophysikalische Chemie, Spektroskopie und Photochemische Kinetik, 37070 Göttingen, Germany

Received: December 20, 2000

The photophysical behavior of four *N*-phenylphenanthridinones is investigated as a function of temperature in *n*-hexane and acetonitrile by using photostationary and time-resolved measurements. The fluorescence spectrum of *N*-(*p*-trifluoromethylphenyl)phenanthridinone and the sterically hindered *N*-(2,6-dimethylphenyl)-phenanthridinone (DMPP) consists of a single emission from a locally excited (LE) state, similar to that of *N*-methylphenanthridinone (MP). In these compounds, intersystem crossing (ISC) to the triplet state is the dominant deactivation process of the LE state at room temperature. Dual fluorescence is observed with *N*-phenylphenanthridinone (PP) and *N*-(*p*-methoxyphenyl)phenanthridinone (MOPP), which consists of an LE emission band in the same spectral region as that of MP and a strongly red-shifted intramolecular charge transfer (ICT) band. X-ray crystallography reveals that in PP the phenyl/phenanthridinone dihedral angle equals 80.6°. From the absence of dual emission in the case of DMPP, it is concluded that the ICT state is considerably more planar than the LE state. From solvatochromic measurements, the ICT dipole moments of MOPP (13.7 D) and PP (10.6 D) are determined. These dipole moments are considerably larger values than those of their LE states: 7.8 D (MOPP) and 7.4 D (PP). The observation of double-exponential LE fluorescence decays for PP in *n*-hexane and acetonitrile and for MOPP in *n*-hexane indicates that the ICT reaction is reversible. From measurements of the fluorescence decays as function of temperature, the activation energies and preexponential factors of the reversible LE ↔ ICT reaction are determined, giving ICT stabilization enthalpies for PP of −0.9 kcal/mol in *n*-hexane and −1.5 kcal/mol in acetonitrile and of −2.4 kcal/mol for MOPP in *n*-hexane. The ICT lifetime τ'_0 of PP and MOPP is unusually short (subnanosecond). For PP in *n*-hexane and acetonitrile, ISC is the main deactivation channel of the ICT state, whereas with MOPP IC is a more effective ICT deactivation process than ISC, especially in acetonitrile in which τ'_0 (28 ps at 20 °C) is completely dominated by IC. The IC is assumed to occur via a conical intersection, brought about by the planarization of the strongly twisted LE state during the ICT reaction of PP and MOPP.

Introduction

Perhaps the best known example of a dual fluorescent molecule is 4-(dimethylamino)benzonitrile (DMABN). Since the discovery of its dual fluorescence in 1959, it was recognized that DMABN emits from two different singlet excited states, a locally excited (LE) state and an intramolecular charge transfer (ICT) state.[1] Several models have been developed to characterize this charge-transfer process and, in particular, the molecular structure of the ICT state.[2−6] In the "twisted intramolecular charge transfer" (TICT) model, it was postulated that DMABN, considered to be planar in the ground state, undergoes a twisting motion in the singlet excited state: a rotation of the dimethylamino group with respect to the phenyl ring toward a perpendicular configuration.[2] In this TICT state, the dimethylamino group was assumed to be electronically decoupled from the benzonitrile moiety. In the "planar intramolecular charge transfer" (PICT) model, on the contrary, it was suggested that the ICT state of DMABN has an essentially planar structure.[3−6] This model was based on experimental evidence, which showed that in the ICT state the amino and benzonitrile groups are not decoupled and that the configurational change of the amino nitrogen from pyramidal toward planar is an important reaction coordinate in the ICT reaction.[3]

In previous publications,[7,8] the photophysical properties of *N*-substituted derivatives of 1,2-, 2,3- and 1,8-naphthalimides have been discussed. Significant differences were found in the excited-state behavior of the *N*-alkyl[7] as compared with the *N*-phenyl[8] compounds. In contrast to the *N*-alkyl derivatives, the singlet excited *N*-phenylnaphthalimides exhibit very efficient internal conversion from the singlet excited state to the ground state and several of these compounds emit dual fluorescence.[8] This dual emission consists of a short-wavelength (SW) fluorescence band from the LE state, in the same spectral region as that of the *N*-alkylnaphthalimides, and a strongly red-shifted long-wavelength (LW) fluorescence emitted by the ICT state. Phenanthridinone and its *N*-methyl derivative were previously studied by Val'kova and co-workers.[9] Dual luminescence was also found for benzanilides, which are structurally related to the phenanthridinones.[10]

* To whom correspondence should be addressed. E-mail: demeter@chemres.hu.

10.1021/jp004555s CCC: $20.00
Published on Web 04/21/2001

It has been suggested[8d] that the LE and ICT emissions of the *N*-phenylnaphthalimides originate from two different singlet excited states with relaxed molecular configuration and solvent surroundings. In the ground state as well as in the LE state, the dihedral angle between the planes of the phenyl and the imide moieties is close to orthogonal, as a result of steric hindrance. In the formation of the ICT state, the geometrical relaxation is assumed to occur by planarization of the twisted *N*-phenyl group relative to the naphthalimide moiety.[8c] As a consequence of this planar configuration, an extended conjugation between the phenyl and the naphthalimide subunits is attained, which stabilizes the ICT relative to the LE state.

The photophysics of four *N*-phenylphenanthridinones and *N*-methylphenanthridinone (MP) in *n*-hexane and acetonitrile is reported in the present paper. In our investigations of the phenanthridinones, attention is directed to the nature of the fluorescent states as well as to the kinetics and the mechanism of the photophysical processes taking place in these molecules. The structure, names, and acronyms (in brackets) of the phenanthridinones are given below.

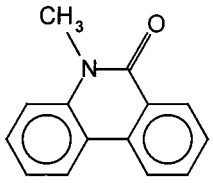

5-methyl-5H-phenanthridin-6-one (MP)

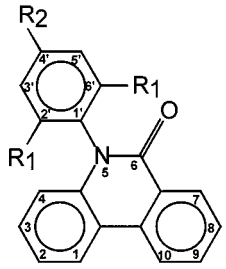

R_1= H, R_2=H : 5-phenyl-5H-phenanthridin-6-one (PP)
R_1= H, R_2= OCH_3 : 5-(4-methoxyphenyl)-5H-phenanthridin-6-one (MOPP)
R_1= H, R_2= CF_3 : 5-(4-trifluoromethylphenyl)-5H-phenanthridin-6-one (TFPP)
R_1=CH_3, R_2=H : 5-(2,6-dimethylphenyl)-5H-phenanthridin-6-one (DMPP)

Experimental Section

Experimental Techniques. Absorption spectra were obtained by using a HP 8452a spectrometer. Fluorescence spectra were recorded with a homemade photon-counting spectrofluorimeter equipped with a Princeton Applied Research 1140 A/B detection system and a red-sensitive photomultiplier (RCA 928). The excitation wavelengths were 334 and 312 nm. In some of the spectra, the occurrence of the second harmonics of the SW fluorescence and the excitation light disturbed the measurements. In these cases, the spectra were measured with and without a 455 nm cutoff filter placed in front of the monochromator. The two spectra were then combined; the short wavelength part was taken from the measurement made without the cutoff filter, and the long wavelength part was obtained from the measurement carried out with cutoff filter. A correction for the reflectance and transmittance of the filter was applied. Combination of the two parts of the spectrum was made around 500 nm, where the spectra could be measured without problem.

The picosecond fluorescence decay measurements were made with a system consisting of an argon ion laser (Coherent Innova 100-10), a dye laser (Coherent 702-1CD, DCM), and a frequency doubler ($LiIO_3$, 325 nm).[11] The fluorescence and scatter records were detected with a Hamamatsu R2803U-07 or R3803U MCP photomultiplier. The instrument response function had a width of ~27 ps at the excitation wavelength. The analysis of the fluorescence decays was carried out by using the method of modulating functions, extended by global analysis.[12,13]

The triplet yields were measured at room temperature, employing the energy transfer method with 9,10-dichloroanthracene or perylene as energy acceptor, by using a Lambda Physik EMG 101 excimer laser (308 nm excitation wavelength). Benzophenone, with a triplet yield of 1.00 in acetonitrile,[14] and *N*-methyl-1,8-naphthalimide ($\Phi_{ISC} = 0.95$ in *n*-hexane)[15] were used as reference compounds. Triplet yields at other temperatures were determined by comparing (immediately after excitation) the transient absorption signal obtained at a given temperature with that measured at 25 °C. The change with temperature in the optical density of the sample was taken into account. Triplet−triplet absorption measurements were carried out at the shoulder (410 nm) of the T−T absorption spectrum.[15]

Materials. MP was prepared as described in the literature.[16] N-phenylphenanthridinone (PP) was obtained by a procedure involving a photochemical rearrangement.[17] The preparation and characterization of MOPP, TFPP, and DMPP is available as Supporting Information.

All compounds were crystallized from chloroform or from an *n*-hexane/ethyl acetate mixture. Further purification was carried out by preparative thin-layer chromatography (Merck PLC Silica Gel) with chloroform or an *n*-hexane/ethyl acetate mixture as the eluent. In the case of PP and MOPP, HPLC was the final purification step. Acetonitrile and *n*-hexane (Uvasol) were purchased from Merck. All other solvents and the compounds used in the synthesis were obtained from Aldrich. The solvents were purified by column chromatography over Al_2O_3.

Results and Discussion

Molecular Structure of PP. The molecular structure and in particular the phenyl/phenanthridinone dihedral angle θ of PP was studied by X-ray crystallography.[18] The phenanthridinone moiety of PP was found to be practically planar. The dihedral angle θ equals 80.6°, in good agreement with the result (89.8°) of DFT(B3LYP)SVP calculations.[19] In accordance with this result, the *N*-aryl bond length was 1.448 Å, not much shorter than the length of a CN single bond (e.g., 1.477 Å in CH_3-NH_2).[20] From the data on the molecular structure of PP presented here, it is concluded that steric hindrance to phenyl group rotation in the *N*-phenylphenanthridinones leads to a nearly perpendicular structure in the ground state, similarly to that found for the *N*-arylnaphthalimides[21].

Absorption and Fluorescence Spectra. The absorption and fluorescence spectra of the five phenanthridinones MP, DMPP, PP, MOPP, and TFPP in *n*-hexane at room temperature are shown in Figure 1. The vibrational structure of the absorption spectra in this solvent is more clearly resolved than in other more polar solvents. All compounds in Figure 1 have similar absorption spectra with a main absorption peak around 30 900 cm^{-1}, which means that the spectrum does not depend strongly on the nature of the N substituent. The lowest-energy peak, corresponding to the $S_0 \rightarrow S_1$ transition, is therefore mainly associated with the phenanthridinone part of the molecules. The energies $E(S_1)$ of the lowest excited singlet state S_1 of the five phenanthridinones in *n*-hexane and acetonitrile, obtained from the crossing points of the absorption and fluorescence spectra, see Figure 1 for *n*-hexane, are listed in Table 1.

TABLE 1: Energy $E(S_1)$ and Yields Φ_i of Five Phenanthridinones in *n*-Hexane and Acetonitrile at 20 °C[a]

	MP		DMPP		PP		TFPP		MOPP	
	n-hexane	acetonitrile	*n*-hexane	acetonitrile	*n*-hexane	acetonitrile	*n*-hexane	acetonitrile	*n*-hexane	acetonitrile
$E(S_1)/cm^{-1}$	29320	29030	29330	29210	29300	28980	29300	29200	29200	28870
Φ_f	0.056	0.059	0.069	0.067	0.033[b]	0.025[b]	0.028	0.043	0.017[b]	0.0019[b]
Φ_{ISC}	0.96	0.94	0.92	0.93	0.91	0.48	0.90	0.93	0.18	0.034
Φ_{IC}		<0.01	0.01	<0.01	0.06	0.50	0.07	0.03	0.80	0.96

[a] The subscript i of the yields Φ_i refers to fluorescence (*f*), intersystem crossing (ISC) and internal conversion (IC). See text for the abbreviations used for the phenanthridinone compounds. [b] $\Phi_f = \Phi_f(LE) + \Phi_f'(ICT)$; see Table 2.

TABLE 2: Fluorescence Maxima $\tilde{\nu}_f^{max}$ and Fluorescence Quantum Yields Φ_f at 20 °C of the LE and ICT States for PP and MOPP in Eight Solvents Spanning the Polarity Scale

	PP					MOPP				
solvent	$\tilde{\nu}_f^{max}/cm^{-1}$	$\Phi_f(LE)$	$\tilde{\nu}_f^{max}/cm^{-1}$	$\Phi'_f(ICT)$	Φ'_f/Φ_f	$\tilde{\nu}_f^{max}/cm^{-1}$	$\Phi_f(LE)$	$\tilde{\nu}_f^{max}/cm^{-1}$	$\Phi'_f(ICT)$	Φ'_f/Φ_f
n-hexane	26 460	0.030	19 440	0.0033	0.11	26 210	0.0040	17 910	0.013	3.3
di-*n*-hexyl ether	26 420	0.031	19 350	0.0037	0.12	26 200	0.0029	17 360	0.0063	2.2
di-*n*-butyl ether	26 390	0.028	18 460	0.0074	0.26	25 980	0.0021	16 910	0.0062	2.9
diethyl ether	26 360	0.031	18 320	0.0102	0.33	26 200	0.0014	16 840	0.0023	1.6
tetrahydrofuran	26 100	0.025	18 300	0.0086	0.34	26 120	0.0012	16 010	0.0014	1.2
n-heptyl cyanide	26 170	0.025	18 180	0.0074	0.30	26 120	0.0030	15 990	0.0010	0.33
n-propyl cyanide	26 140	0.021	17 820	0.0067	0.32	26 100	0.0017	15 680	0.0007	0.41
acetonitrile	26 090	0.019	17 560	0.0063	0.33	26 000	0.0015	14 810	0.0004	0.27

Fluorescence Spectra. The fluorescence spectra of MP, DMPP, and TFPP in *n*-hexane (Figure 1) consist of a single LE emission band. This band shows mirror symmetry with the structured absorption spectrum. With PP and MOPP dual fluorescence is observed, with an ICT emission band strongly red-shifted with respect to the LE fluorescence. The ICT band shape was determined from the best fit between the measured fluorescence spectrum of PP or MOPP and the fluorescence spectrum of TFPP (taken as the model compound for the LE fluorescence) plus a Gaussian curve representing the ICT fluorescence. Similar results were obtained with an alternative procedure, in which the spectrum of the model compound TFPP is subtracted from the measured spectrum.

Quantum Yields of Fluorescence, ISC, and IC in *n*-Hexane and Acetonitrile. With the three phenanthridinones MP, DMPP, and TFPP, dual fluorescence could not be detected, neither in the nonpolar solvent *n*-hexane (Figure 1) nor in the polar acetonitrile. The LE fluorescence quantum yield $\Phi_f(LE)$ of these molecules at room temperature has values between 0.03 (TFPP) and 0.07 (DMPP), see Table 1, in *n*-hexane as well as in acetonitrile. The main deactivation process of the LE state is intersystem crossing (ISC), with triplet yields between 0.90 and 0.96 at room temperature (Table 1). Similar large triplet yields were obtained at low as well as at high temperatures. Internal conversion to the S_0 ground state is absent or weak (MP and DMPP) or of minor importance (TFPP). With TFPP, however, Φ_{ISC} decreases with increasing temperature accompanied by an increase in Φ_{IC}. All of the deactivation processes of LE fluorescence, ISC, and IC do not strongly depend on solvent polarity (Table 1).

With PP in *n*-hexane, showing dual fluorescence with a relatively weak contribution from the ICT state (Figure 1 and Table 2), ISC is the main deactivation channel, with the overall yields $\Phi_{ISC} = 0.91$ and $\Phi_{IC} = 0.06$ (Table 1). For PP in acetonitrile, however, the increase in the efficiency of the ICT reaction (Figure 2 and Table 2) is accompanied with a decrease in total triplet yield and a strong increase in the IC yield, $\Phi_{ISC} = 0.48$ and $\Phi_{IC} = 0.50$, see Table 1. With MOPP, which is more clearly dual fluorescent in *n*-hexane than PP (Figures 1 and 2 and Table 2), the increase in Φ_{IC} at the expense of Φ_{ISC} associated with an increasing efficiency of the ICT reaction is strongly enhanced as compared with PP. As seen in Table 1, IC has become the major deactivation process for MOPP in acetonitrile at room temperature, with yields $\Phi_{IC} = 0.95$ and $\Phi_{ISC} = 0.03$. The triplet yield of both dual luminescent compounds PP and MOPP decreases slightly with increasing temperature. The results described in this section show that the major ISC deactivation channel of the single fluorescent phenanthridinones MP, DMPP, and TFPP is replaced by IC when the ICT reaction sets in.

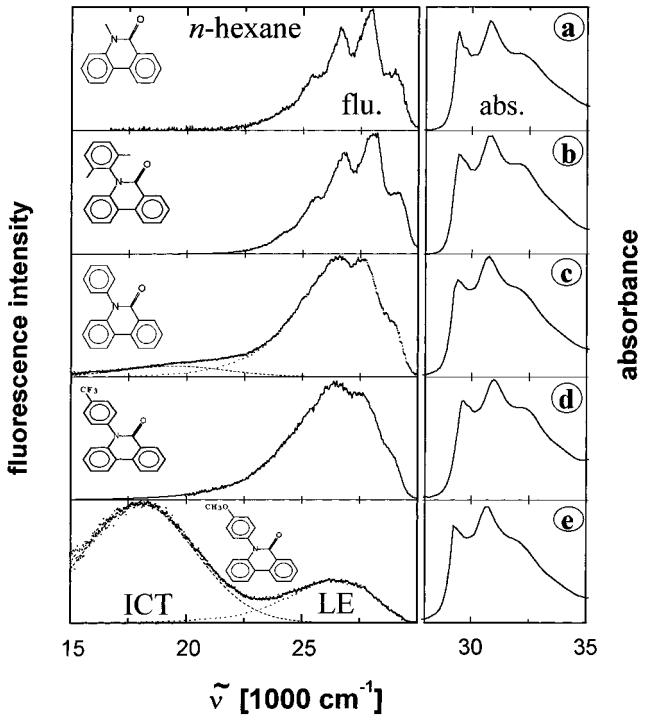

Figure 1. Absorption and fluorescence spectra of (a) MP, (b) DMPP, (c) PP, (d) TFPP, and (e) MOPP in *n*-hexane at room temperature. For the dual fluorescent compounds PP and MOPP: experimental fluorescence spectrum (●), model spectrum TFPP (···), difference spectrum (- --), calculated spectrum (—). See text.

Solvent Polarity Dependence of Dual Fluorescence. PP and MOPP. The emission spectra of the dual fluorescent phenanthridinones PP and MOPP at room temperature in a series of solvents spanning the polarity scale are presented in Figure 2.

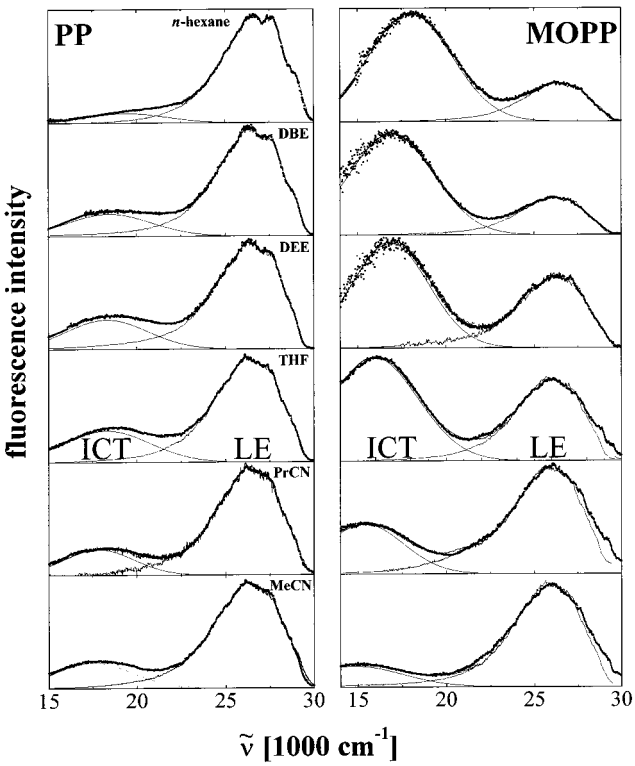

Figure 2. Fluorescence spectra of PP (left) and MOPP (right) in different solvents at room temperature (top to bottom: *n*-hexane, dibutyl ether, diethyl ether, tetrahydrofuran, butyronitrile, and acetonitrile). See caption of Figure 1.

The emission spectrum of TFPP was again used as a model for the LE fluorescence. A comparison of these spectra shows that the fluorescence of PP and MOPP clearly depends on solvent polarity. With PP, the LE fluorescence is dominant in all solvents. The ICT/LE fluorescence quantum yield ratio Φ′(ICT)/Φ(LE) increases from *n*-hexane to diethyl ether and remains more or less constant upon further increase of solvent polarity, see Table 2. In the case of MOPP, in contrast, the ICT fluorescence dominates in *n*-hexane and the ratio Φ′(ICT)/Φ(LE) decreases with increasing solvent polarity from *n*-hexane to acetonitrile (Table 2).

Solvatochromic Measurements. Solvatochromic measurements were carried out to determine the LE and ICT dipole moments of the phenanthridinones. In this manner, the extent of charge-transfer taking place during the ICT reaction of these molecules can be established. The solvent polarity dependence of the energy of the maxima of the LE and ICT fluorescence bands is described by eqs 1 and 2.[22−24]

$$\tilde{\nu}_f^{LE} = \frac{-1}{4\pi\pi_0}\frac{2}{hc\rho^3}\mu_e^{LE}(\mu_e^{LE} - \mu_g^{FC})(f - f') + \text{constant} \quad (1)$$

$$\tilde{\nu}_f^{ICT} = \frac{-1}{4\pi\pi_0}\frac{2}{hc\rho^3}(\mu_e^{ICT} - \mu_g^{FC'})^2\left(f - \frac{1}{2}f'\right) + \text{constant} \quad (2)$$

In these equations, ρ is the equivalent spherical radius of the solute (Onsager radius), and ϵ_0 is the vacuum permittivity of the solvent; μ_e(LE) and μ_e(ICT) are the dipole moments of the LE and ICT states, respectively, whereas μ_g^{FC}(LE) and μ_g^{FC}(ICT) represent the dipole moments of the Franck−Condon (FC) ground states reached upon emission from the LE and ICT states. It is assumed here that μ_g^{FC}(LE) and μ_g^{FC}(ICT) are equal to the ground-state dipole moment μ_g of the relaxed molecules. The solvent polarity parameters $(f - f')$ and $(f - {}^1/_2 f')$ are

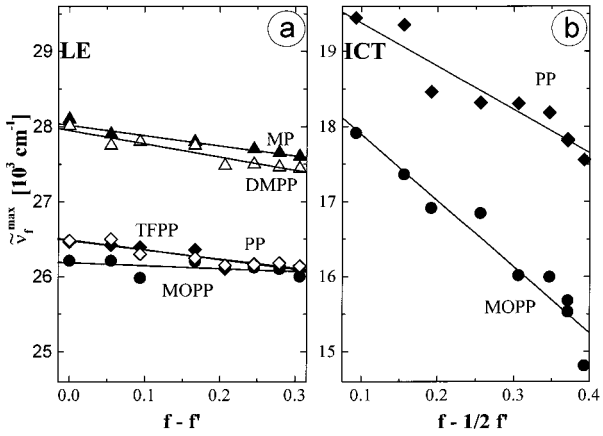

Figure 3. Plot of the wavenumber of the emission maxima $\tilde{\nu}_f^{max}$ of (a) the LE fluorescence versus the solvent polarity parameter $f - f'$ (eq 3) and of (b) the ICT fluorescence versus $f - {}^1/_2 f'$ (eq 4). Data points: MP (▲), DMPP (△), TFPP (◇), PP (◆), and MOPP (●).

TABLE 3: Onsager Radius ρ, Dipole Moments μ_g (Ground State), μ_e^{LE} and μ_e^{ICT}, and Input Parameters (eqs 1 and 2) for Five Phenanthridinones at Room Temperature

			LE band			ICT band		
compounds	ρ /Å	μ_g /D[a]	slope /cm^{-1} [b]	$\Delta\mu_e^{LE}$ /D[c]	μ_e^{LE} /D	slope /cm^{-1} [d]	$\Delta\mu_e^{ICT}$ /D[e]	μ_e^{ICT} /D
MP	4.36	2.87	1810	4.8	7.7			
PP	4.75	2.75	1310	4.6	7.4	5760	7.8	10.6
DMPP	4.91	2.81	1360	4.9	7.7			
MOPP	4.92	3.43	400	4.4	7.8	8830	10.2	13.7
TFPP	5.12	5.47	1225	7.3	12.8			

[a] Calculated ground-state dipole moment. See text. [b] Slope of $\tilde{\nu}_f^{max}$(LE) against $(f - f')$: $\mu_e^{LE}(\mu_e^{LE} - \mu_g)/\rho^3$, see eqs 1 and 3. [c] $\Delta\mu_e^{LE} = \mu_e^{LE} - \mu_g$. [d] Slope of $\tilde{\nu}_f^{max}$(ICT) against $(f - {}^1/_2 f')$: $(\mu_e^{ICT} - \mu_g)^2/\rho^3$, see eqs 2 and 4. [e] $\Delta\mu_e^{ICT} = \mu_e^{ICT} - \mu_g$.

defined by eqs 3 and 4.

$$f - f' = (\epsilon - 1)/(2\epsilon + 1) - (n^2 - 1)/(2n^2 + 1) \quad (3)$$

and

$$f - {}^1/_2 f' = (\epsilon - 1)/(2\epsilon + 1) - {}^1/_2(n^2 - 1)/(2n^2 + 1) \quad (4)$$

where ϵ and n are the dielectric constant and the refractive index of the solvent.

The energies $\tilde{\nu}_f^{max}$ of the LE band of the five phenanthridinones MP, PP, DMPP, TFPP, and MOPP (data for PP and MOPP in Table 2) are plotted in Figure 3a against the solvent polarity function $(f - f')$, whereas in Figure 3b, the energies of the ICT fluorescence maxima of PP and MOPP (Table 2) are plotted versus $(f - {}^1/_2 f')$.[3a]

To derive the dipole moments from the slopes of these plots by using eqs 1 and 2, the ground-state dipole moment μ_g and the Onsager radius ρ must be known. The μ_g values were obtained from AM1 semiempirical calculations.[25a] Such calculations give reasonable results for the structurally related benzanilide and isoquinoline molecules, with 3.58 and 2.24 D as compared with the experimental values 3.60[25b] and 2.73 D,[25b] respectively. The Onsager radius ρ was obtained by adopting[23] a molecular density of 1.00 for the phenanthridinones. The data on ρ and μ_g, as well as the $\Delta\mu$ and μ_e values are presented in Table 3. It is seen that the LE state of the phenanthridinones is moderately polar, with a dipole moment μ_e^{LE} of 7.4 D for PP and 7.8 D for MOPP. The ICT state of these molecules has a considerably larger dipole moment: $\mu_e^{ICT} = 10.6$ D for PP and

TABLE 4: Fluorescence Decay Times τ, Rate Constants $k_i = A_i \exp(-E_i/RT)$ (i = F, ISC, IC) at 20 °C and the Arrhenius Parameters A_i and E_i for the Single Fluorescent Phenanthridinones MP, DMPP, and TFPP

	MP		DMPP		TFPP	
	n-hexane	acetonitrile	*n*-hexane	acetonitrile	*n*-hexane	acetonitrile
τ/ns	0.460	0.435	0.595	0.580	0.240	0.430
$k_f/10^8\ s^{-1}$	1.22	1.36	1.16	1.15	1.17	1.00
$k_{ISC}/10^8\ s^{-1}$	20.9	21.6	15.5	16.0	37.5	21.6
$k_{IC}/10^8\ s^{-1}$	0.0	<0.2	0.2	<0.2	2.9	0.7
$\log(A_{ISC}/s^{-1})$[a]	9.60 ± 0.02	9.60 ± 0.02	9.50 ± 0.02	9.50 ± 0.02	9.59 ± 0.04	9.60 ± 0.02
E_{ISC}/kcal mol^{-1} [a]	0.16 ± 0.04	0.32 ± 0.02	0.40 ± 0.02	0.41 ± 0.02	0.036 ± 0.05	0.31 ± 0.04
$\log(A_{IC}/s^{-1})$ [a]					12.6 ± 0.8	13.2 ± 0.6
E_{IC}/kcal mol^{-1} [a]					5.5 ± 1.0	7.4 ± 0.8

[a] The errors are the two σ values derived from the Arrhenius plots of k_{ISC} and k_{IC} (Figure 5). These errors are to be considered as lower limits.

13.7 D for MOPP. These data show that the appearance of dual fluorescence with PP and MOPP results from an ICT reaction, similar to what has been observed with DMABN.[1−6]

Characterization of the ICT State of PP and MOPP. The presence of the phenyl group in PP and MOPP is essential for the appearance of dual fluorescence in the phenanthridinones, because LE and ICT emission has only been observed for molecules with a phenyl group attached to the nitrogen atom of the phenanthridinone moiety. In addition, the nature of the substituent on this phenyl group exerts a strong influence on the LE→ICT reaction. The ICT fluorescence disappears when the phenyl group is para-substituted by the electron acceptor group CF_3, whereas ICT becomes the dominant fluorescence band for the MOPP compound with the electron donor substituent OCH_3. These observations are a consequence of the charge-transfer character of the ICT state, with a charge displacement from the phenyl to the carbonyl group.

Another important feature of the ICT reaction in the phenanthridinones becomes clear when methyl groups are substituted in the ortho position of the *N*-phenyl ring. As seen from a comparison of the spectra of DMPP and PP in Figure 1, the ortho-methyl substitution completely eliminates the ICT fluorescence. This observation shows that structural relaxation by way of phenyl rotation from a nearly perpendicular toward a coplanar molecular structure (antitwist) occurs during the formation of the ICT state, which can be strongly hindered by the presence of ortho-methyl substituents.

Single-Exponential Fluorescence Decays. MP, DMPP, and TFPP. The picosecond fluorescence decays of MP, DMPP, and TFPP in acetonitrile at 20 °C (see Figure 4 parts a and b) are single exponential, with relatively short decay times of 0.580 and 0.435 ns, see Table 4. For TFPP in acetonitrile at 20 °C, the same decay time was determined at the maximum (380 nm) and at the red edge (500 nm) of the emission band, see Figures 1 and 2. The fluorescence decays of MP, DMPP, and TFPP in *n*-hexane and acetonitrile remain single exponential over the entire temperature range studied, from −90 to +80 C in *n*-hexane and from −40 to +80 °C in acetonitrile. These observations support our conclusion derived from the fluorescence spectra discussed above, that even in the polar solvent acetonitrile an ICT reaction does not occur with MP, DMPP, and TFPP. The decay time τ of these molecules is hence determined by three processes, fluorescence (*f*), ISC, and IC: $\tau^{-1} = (k_f + k_{ISC} + k_{IC})$.

Arrhenius plots of the reciprocal decay times τ^{-1} of MP and DMPP in *n*-hexane and acetonitrile give straight lines, whereas for TFPP, a clear deviation from linearity is found. This is in accord with our previous observation (Table 1) that a single deactivation process (k_{ISC}) dominates the photophysics of MP and DMPP in *n*-hexane and acetonitrile, whereas two reactions (k_{ISC} and k_{IC}) with apparently different activation energies are involved in the deactivation of TFPP.

Rate Constants k_f, k_{ISC}, and k_{IC} of MP, DMPP, and TFPP. From the decay times determined from the single-exponential fluorescence decays of MP, DMPP, and TFPP in *n*-hexane and acetonitrile at 20 °C (Figure 4a,b and Table 4), together with the fluorescence quantum yields Φ_f and the yields of ISC (Φ_{ISC}) and IC (Φ_{IC}) in Table 1, the corresponding rate constants k_i (i = f, ISC, IC) can be obtained via eq 5:

$$k_i = \Phi_i/\tau \tag{5}$$

The results for k_f, k_{ISC} and k_{IC} at 20 °C are presented in Table 4. It can be seen from these data that the relatively short decay times of MP, DMPP, and TFPP are caused by triplet formation (k_{ISC}) as the dominant depopulating process for the LE state in *n*-hexane as well as in acetonitrile. The efficiency of this ISC process (Φ_{ISC} between 0.90 and 0.96; Table 1) may be the result of a nearly thermoneutral $S_1(\pi\pi^*) \rightarrow T_n(n\pi^*)$ reaction. From semiempirical calculations, Val'kova et al.[9b] found an $n\pi^*$ triplet state with an energy of 30 800 cm^{-1} above the ground state, which can be the triplet state that is involved in the ISC process from the S_1 state of the phenanthridinones, having energies $E(S_1)$ between 28 900 and 29 300 cm^{-1} (Table 1).

ISC and IC Arrhenius Parameters for MP, DMPP, and TFPP. From the temperature dependence of the rate constants k_i ($= A_i e^{-Ei/RT}$) of MP, DMPP, and TFPP in *n*-hexane and acetonitrile, see Figure 5 for TFPP, the preexponential factors A_i and the activation energies E_i (i = ISC, IC) were obtained (Table 4). The ISC activation energy E_{ISC} of the investigated phenanthridinones is small, with values around 0.3 kcal/mol. This indicates that the two states S_1 and T_n involved in the ISC process are close in energy, leading to an estimation of the energy of the triplet state involved in the ISC process of around 29 400 cm^{-1}. This value is somewhat lower than the $T_n(n\pi^*)$ energy (30 800 cm^{-1}) reported by Val'kova et al.,[9] as mentioned above.

Whereas the three single fluorescent compounds MP, DMPP, and TFPP undergo similar photophysical processes at room temperature, with dominant ISC and relatively unimportant IC reactions (Table 4), this similarity disappears at higher temperatures. For MP and DMPP, intersystem crossing continues to be a more efficient process than internal conversion, as seen from the Arrhenius parameters in Table 4. With TFPP, the significant temperature dependence of the internal conversion (k_{IC} in Figure 5, see Table 4) makes this process comparable in importance with intersystem crossing at higher temperatures. The larger efficiency of the thermally activated internal conversion observed for TFPP, as compared with MP and DMPP, may be caused by vibronic interaction between the two close-lying $n\pi^*$ and $\pi\pi^*$ states,[26,27] a proximity effect.[28]

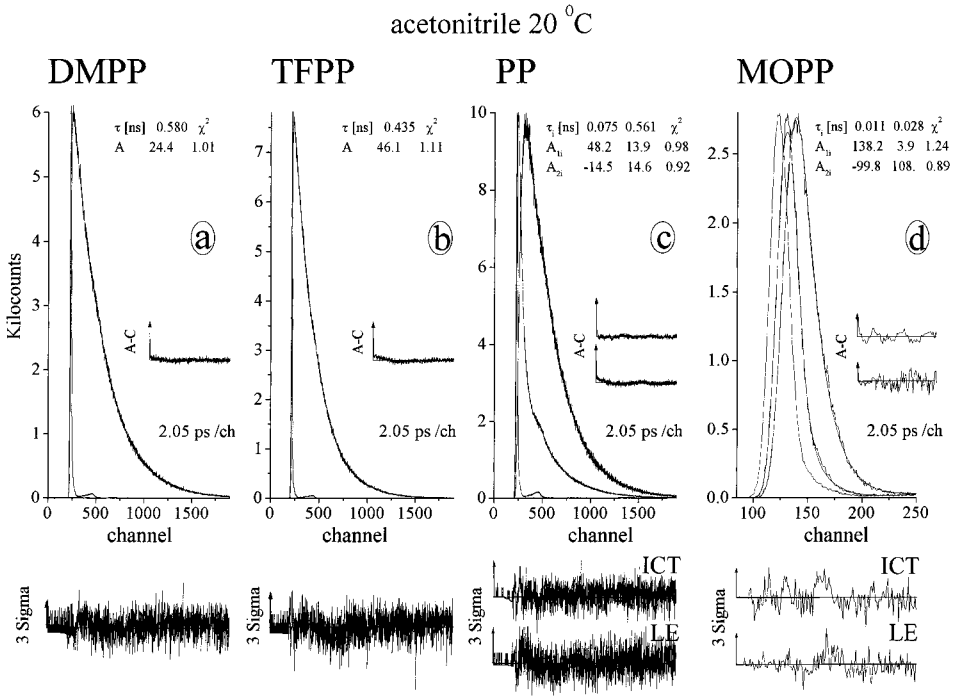

Figure 4. Fluorescence response functions of (a) DMPP, (b) TFPP, (c) PP, and (d) MOPP in acetonitrile at 20 °C. The fluorescence decays of DMPP and TFPP were measured at 380 nm. The LE (at 375 nm) and ICT (at 540 nm) decays of PP and MOPP are analyzed simultaneously (global analysis). The decay times (τ) and the preexponential factors (A) are given, see eqs 6 and 7 for PP and MOPP. The weighted deviations, expressed in σ (expected deviation), the autocorrelation functions A−C, and the χ^2 values are also indicated.

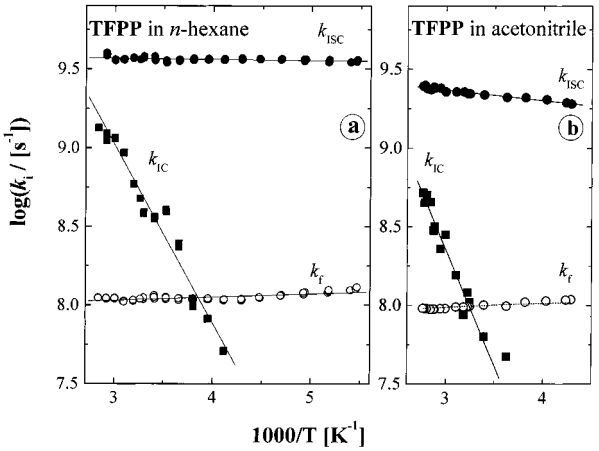

Figure 5. Arrhenius plots of the rate constants k_f (fluorescence), k_{ISC} (intersystem crossing), and k_{IC} (internal conversion) for TFPP in *n*-hexane (a) and acetonitrile (b). The solid lines through the data points for k_{ISC} and k_{IC} are fits to the experimental data. For the fluorescence, an average k_f value was employed, which was made temperature dependent by using the temperature dependence of the refractive index of the solvent.

Double Exponential Fluorescence Decays. PP and MOPP. Fluorescence decay curves of the dual fluorescent compounds PP and MOPP were measured in the LE and ICT parts of the spectrum at wavelengths where interference from overlapping LE and ICT fluorescence bands does not occur, see Figure 4 parts c and d (acetonitrile) and Figure 6 (*n*-hexane). The LE and ICT fluorescence decays i_f(LE) and i_f(ICT) are double exponential (eqs 6 and 7):

$$i_f(\mathrm{LE}) = A_{11}e^{-t/\tau_1} + A_{12}e^{-t/\tau_2} \quad (6)$$

$$i_f(\mathrm{ICT}) = A_{21}e^{-t/\tau_1} + A_{22}e^{-t/\tau_2} \quad (7)$$

The amplitude ratio A_{22}/A_{21} (eq 7) for the ICT fluorescence

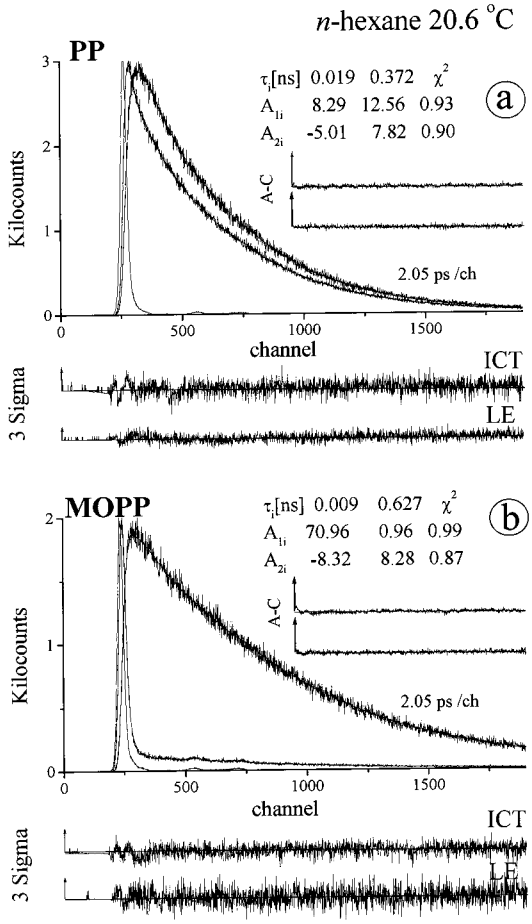

Figure 6. Fluorescence response functions of (a) PP and (b) MOPP in *n*-hexane at 20.6 C. The LE (at 370 nm) and ICT (at 500 nm) decays are analyzed simultaneously (global analysis). See the caption of Figure 4.

TABLE 5: Data for the Radiative and Nonradiative Photophysical Processes of the Dual Fluorescent Phenanthridinones PP and MOPP in *n*-Hexane and Acetonitrile[a]

	PP		MOPP	
	n-hexane	acetonitrile	*n*-hexane	acetonitrile
τ_2/ns	0.019	0.075	0.009	0.011
τ_1/ns	0.372	0.561	0.627	0.028
$A = A_{12}/A_{11}$ (eq 11)	0.66	3.47	73.9	
τ_0'/ns	0.29	0.62	0.63	0.028
$k_a/10^9\ s^{-1}$	20.4	8.45	107.5	88.6
$k_d/10^9\ s^{-1}$	29.3	2.74	1.5	
$\log(A_a/s^{-1})$[b]	11.60 ± 0.18	12.03 ± 0.08	11.88 ± 0.12	12.16 ± 0.28
E_a/kcal mol^{-1} [a]	1.8 ± 0.2	2.8 ± 0.1	1.2 ± 0.1	1.7 ± 0.4
$\log(A_d/s^{-1})$[a]	12.67 ± 0.08	12.69 ± 0.04	11.90 ± 0.07	
E_d/kcal mol^{-1} [a]	2.9 ± 0.2	4.3 ± 0.1	3.6 ± 0.2	
ΔH/kcal mol^{-1} [a]	-0.9 ± 0.4	-1.5 ± 0.2	-2.4 ± 0.3	

	LE	ICT	LE	ICT	LE	ICT	LE	ICT
Φ_f(LE), Φ'_f(ICT)	0.030	0.0033	0.019	0.0063	0.004	0.013	0.0015	0.0004
Φ_{ISC}(LE), Φ'_{ISC}(ICT)	0.48[c]	0.43	0.40[c]	0.08	0.04[c]	0.14	0.024[c]	0.010
Φ_{IC}(LE), Φ'_{IC}(ICT)		0.06		0.49		0.80		0.96
k_f, $k_f'/10^8 s^{-1}$	1.3	0.23	1.0	0.18	2.3	0.21	1.4	0.15
k_{ISC}, $k'_{ISC}/10^9 s^{-1}$	2.09[d]	3.0	2.16[d]	0.22	2.09[d]	0.23	2.16[d]	0.37
k_{IC}, $k'_{IC}/10^9 s^{-1}$		~0.4		1.4		1.34		35

[a] The decay times, rate constants and yields given in the table are the values derived from the room temperature (20 °C) measurements shown in Figures 4 and 6. [b] The errors are the two σ values derived from the Arrhenius plots given in Figures 7 and 8. These errors are to be considered as lower limits. [c] Values derived by assuming that k_{ISC}(LE) is the same as for the model compound MP (see text). [d] Values taken from the model compound MP.

response functions has a value close to −1.0 for PP and MOPP in both solvents. This means that the ICT state cannot be reached directly by light absorption from the ground state but originates from the primarily excited LE state as its precursor, as shown in Scheme 1. A similar situation has been shown to occur with DMABN.[3]

Mechanism of ICT Reaction of PP and MOPP. In Scheme 1, k_a and k_d are the forward and backward ICT reactions. τ_0 and τ'_0 designate the fluorescence lifetimes of the LE and ICT states.

For Scheme 1, eqs 8−11 hold:[29]

$$\frac{1}{\tau_{1,2}} = \frac{1}{2}\{(X + Y) \mp [(X - Y)^2 + 4k_a k_d]^{1/2}\} \qquad (8)$$

where

$$X = k_a + 1/\tau_0 \qquad (9)$$

and

$$Y = k_d + 1/\tau'_0 \qquad (10)$$

For the preexponential factors A_{1i} and A_{2i} in eqs 6 and 7, the following expressions are valid:

$$A = \frac{A_{12}}{A_{11}} = \frac{(X - 1/\tau_1)}{(1/\tau_2 - X)} \qquad (11)$$

$$\frac{A_{22}}{A_{21}} = -1 \qquad (12)$$

ICT Rate Constants and Lifetime of Dual Fluorescent PP and MOPP at 20 °C. From the decay parameters τ_1, τ_2, and A, together with the lifetime τ_0 of the model compound MP (Table 4), the kinetic parameters k_a, k_d, and τ'_0 (Scheme 1) for PP and MOPP in *n*-hexane (Figure 6) and acetonitrile (Figure 4 parts c and d) at around 20 °C were calculated by using eqs 8−11. The results are listed in Table 5. For MOPP in *n*-hexane, the

SCHEME 1

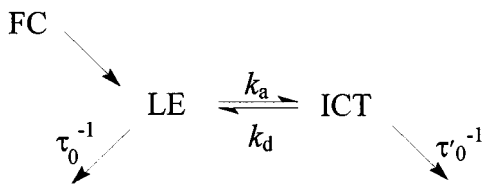

ICT rate constant k_a ($108 \times 10^9\ s^{-1}$) is considerably larger than for PP ($20 \times 10^9\ s^{-1}$), in accord with the larger efficiency, as deduced from the ratio Φ'(ICT)/Φ(LE) (Figure 1, Table 2) of the ICT reaction in MOPP as compared with PP. The thermal back reaction k_d in *n*-hexane is smaller for MOPP ($1.5 \times 10^9\ s^{-1}$) than for PP ($29 \times 10^9\ s^{-1}$), indicating that the enthalpy difference $-\Delta H$ between the LE and ICT states (Scheme 1) is larger for MOPP than for PP (see below and Table 5), as expected on the basis of the larger ICT efficiency observed for the former compound.

In acetonitrile (Figure 4 parts c and d and Table 5), the forward ICT rate constant k_a of MOPP ($89 \times 10^9\ s^{-1}$) likewise is larger than that of PP ($8.5 \times 10^9\ s^{-1}$). The ICT → LE rate constant k_d of MOPP in acetonitrile cannot be determined, as the longer decay time τ_1 of the LE emission (Figure 4d) is attributed to an impurity. This conclusion is based on the observation that the contribution of τ_1 to the LE decay of MOPP is already small in the slightly polar diethyl ether ($A = 260$, eq 11) and will be reduced further with increasing solvent polarity. These results indicate that for MOPP in acetonitrile the condition $k_d \ll 1/\tau'_0$ holds (Scheme 1).[3]

An important feature of the photophysics of MOPP in acetonitrile is the large IC yield ($\Phi_{IC} = 0.95$; Table 1). The unusually short ICT lifetime τ'_0 (28 ps; Figure 4d and Table 5) of MOPP in this solvent is due to a dominating IC process originating from the ICT state (Table 5), as will be further discussed below. The lifetime τ'_0 gradually shortens with increasing solvent polarity, from 630 ps in *n*-hexane (Table 5) to 28 ps in acetonitrile.[30]

Arrhenius plots for PP and MOPP. The LE and ICT

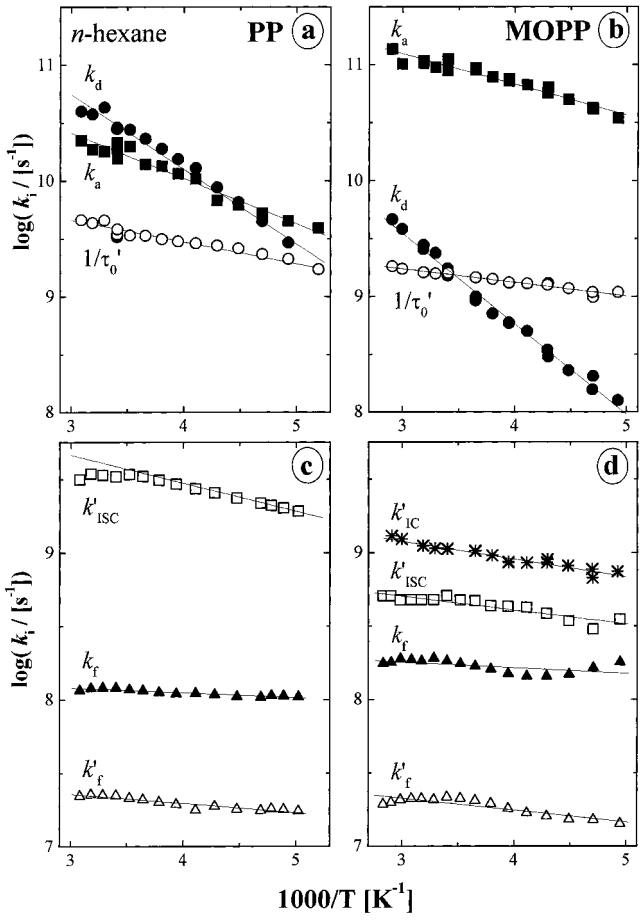

Figure 7. Arrhenius plots of the reciprocal ICT lifetime $1/\tau'_0$ (○) and the forward and backward ICT rate constants k_a (■) and k_d (●) given in *n*-hexane for PP (a) and MOPP (b). In addition, the Arrhenius plots for k_f (s), k'_f (▲), k'_{ISC} (△), and k'_{IC} (*) are shown in insets (c) and (d) for PP and MOPP, respectively.

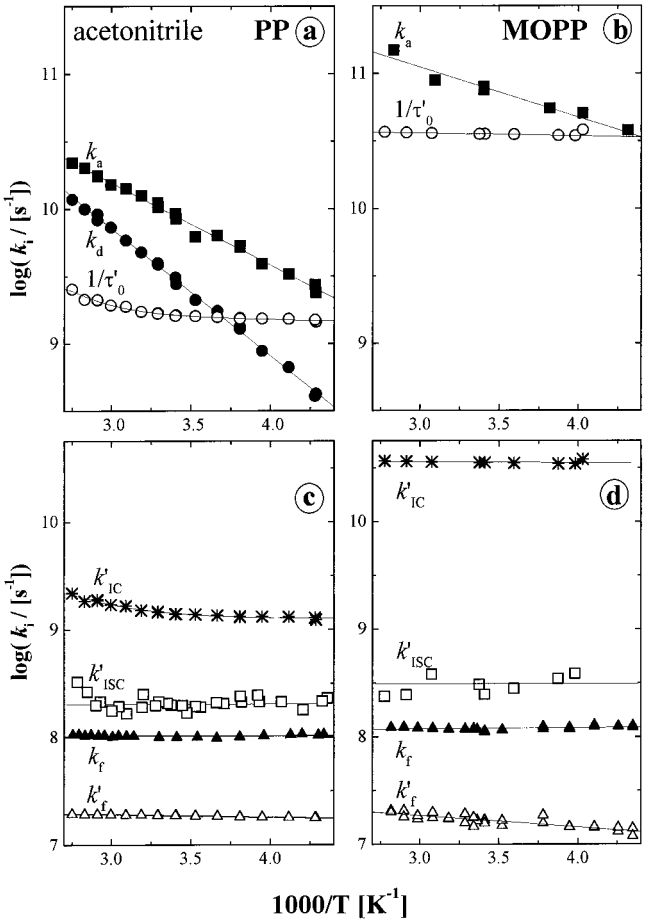

Figure 8. Arrhenius plots of photophysical rate parameters determined for PP (a and c) and MOPP (b and d) in acetonitrile. For designations, see caption of Figure 7.

fluorescence decays of PP and MOPP were measured as a function of temperature in *n*-hexane and acetonitrile. Arrhenius plots of k_a, k_d, and $1/\tau'_0$ resulting from these measurements are presented in Figure 7 (*n*-hexane) and Figure 8 (acetonitrile). The activation energies and the preexponential factors of the forward (E_a and A_a) and backward (E_d and A_d) ICT reactions are listed in Table 5.

From the activation energies E_a and E_d, the following ICT reaction enthalpies ΔH ($= E_a - E_d$), see Figure 9, are obtained for PP: −1.1 kcal/mol in *n*-hexane and −1.5 kcal/mol in the more polar acetonitrile solvent (Table 5). For MOPP in *n*-hexane, the ICT state is more strongly stabilized relative to LE ($\Delta H = -2.4$ kcal/mol) than is the case for PP. This result is in accord with the larger ICT efficiency of the former molecule.

FC Repulsion Energies δE_{FC}. Information on the structural changes taking place during an ICT reaction can be obtained from the energy difference δE_{FC} between the Franck−Condon (FC) state reached upon emission from the ICT state and the equilibrated ground state, see Figure 9. From the known values of ΔH (Table 5), the singlet energies $E(S_1)$ (Table 1) and the energies of the ICT emission maxima $h\tilde{\nu}_f^{ICT}$ (Table 2), energies δE_{FC} in *n*-hexane of 27.3 kcal mol^{-1} for PP and 29.9 kcal mol^{-1} for MOPP are determined. The δE_{FC} energies obtained for PP and MOPP are significantly larger than those reported in the literature for DMABN[31] (16.3 kcal mol^{-1} in toluene) or 9-cyano-10-(dimethylamino)-anthracene[32] (12.7 kcal mol^{-1} in butyronitrile). The larger δE_{FC} values found for PP and MOPP indicate that significant structural relaxation, such as phenyl group rotation toward planarity and bond length changes, takes place in PP and MOPP during the LE → ICT reaction.

Radiative Rate Constants k_f(LE) and k'_f(ICT). The separate radiative rate constants k_f(LE) and k'_f(ICT) can be determined from the LE and ICT fluorescence quantum yields Φ(LE) and Φ′(ICT) listed in Table 2 by using eqs 13 and 14,[31] which are derived by applying the steady-state approximation (Scheme 1):

$$k_f(\mathrm{LE}) = \Phi_f(\mathrm{LE})\,\frac{k_a\tau'_0{}^{-1} + k_d\tau_0{}^{-1} + \tau_0{}^{-1}\tau'_0{}^{-1}}{k_d + \tau'_0{}^{-1}} \quad (13)$$

and

$$k'_f(\mathrm{ICT}) = \Phi'_f(\mathrm{LE})\,\frac{k_a\tau'_0{}^{-1} + k_d\tau_0{}^{-1} + \tau_0{}^{-1}\tau'_0{}^{-1}}{k_a} \quad (14)$$

In *n*-hexane and acetonitrile, the radiative rate constant k_f(LE) is between 6 (PP) and 10 (MOPP) times larger than k'_f(ICT) (Table 5), similar to what has been observed with DMABN.[3,5,31] From the data presented in Figures 8 parts a and b, it is seen that k_f(LE) slightly decreases with increasing temperature for both compounds. This effect is attributed to the temperature dependence of the refractive index n_D of the solvent.[33] However, k'_f(ICT) as well as k'_f(ICT)/n_D^2 increase with increasing temperature. After taking into account[34] the temperature dependence of the refractive index, apparent activation energies of about

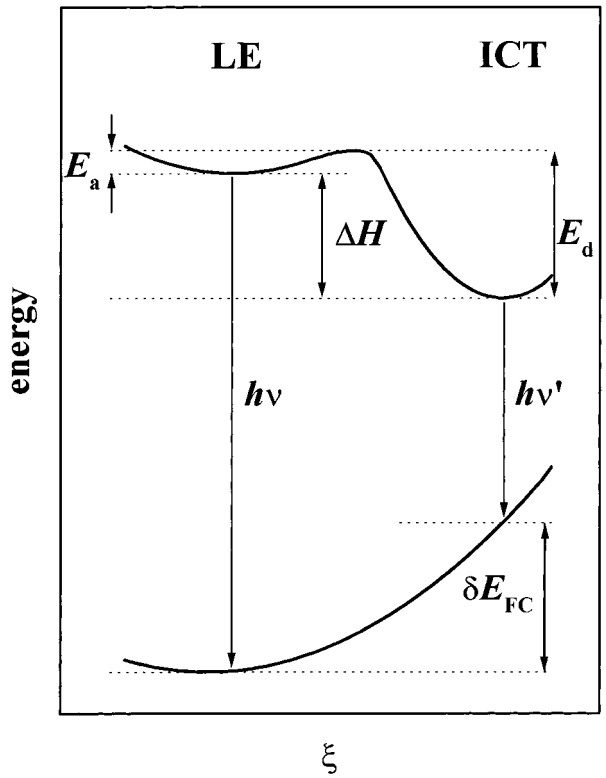

Figure 9. Schematic potential energy diagram describing the LE ↔ ICT reactions and the fluorescence emission from the LE and ICT states of the phenanthridinones PP and MOPP. ξ represents a complex coordinate, involving structural changes (twisting around the N-phenyl bond and bond length changes) and solvent relaxation. E_a and E_d are the activation energies and $\Delta H = E_a - E_d$ is the enthalpy change in the LE ↔ CT reaction. δE_{FC} is the energy difference between the Franck−Condon state reached upon emission from the ICT state and the equilibrated ground state.

0.1 and 0.4 kcal mol^{-1} are obtained for k'_f(ICT) of PP and MOPP, respectively. A similar temperature dependence has been observed for k'_f(ICT) of DMABN in toluene,[31] as well as for the radiative rate constant k_f of a number of 1-aminonaphthalenes in acetonitrile.[33] The phenomenon was explained by the possibility, that an admixture of two or more excited states is involved in the fluorescence emission and that the relative contribution from these states changes with temperature.[33]

Stevens-Ban Plot of Φ_f'(ICT)/Φ_f(LE). For the dual fluorescent PP in acetonitrile, a plot of ln(Φ_f'(ICT)/Φ_f(LE)) versus the reciprocal absolute temperature is presented in Figure 10. Such a Stevens-Ban plot[35] is characteristic for a system undergoing a reversible reaction in the excited state, such as here between LE and ICT (Scheme 1), see eq 15. For MOPP in acetonitrile, only the low-temperature branch ($k_d \ll 1/\tau'_0$) of the Φ_f'(ICT)/Φ_f(LE) plot can be determined, because of its strongly stabilized ICT state, as discussed above (Table 5):

$$\frac{\Phi'(\mathrm{ICT})}{\Phi(\mathrm{LE})} = \frac{k'_f \cdot [\mathrm{ICT}]}{k_f \cdot [\mathrm{LE}]} = \frac{k'_f}{k_f} \cdot \frac{k_a}{k_d + 1/\tau'_0} \qquad (15)$$

Curve fitting of the Φ_f'(ICT)/Φ_f(LE) data in Figure 10, with the assumption that k_f'/k_f and τ'_0 (eq 15) do not depend on temperature (full line), results in ICT activation energies E_a = 2.5 kcal/mol and E_d = 3.9 kcal/mol. These data are in good agreement with those (E_a = 2.8 kcal/mol and E_d = 4.3 kcal/mol) derived from the time-resolved measurements (Table 5). The maximum of Φ′(ICT)/Φ(LE) in Figure 10 occurs at ∼20 °C, in accord with the finding (Table 5) that the condition $k_d = 1/\tau'_o$ required for this maximum[3a] is reached at this temperature.

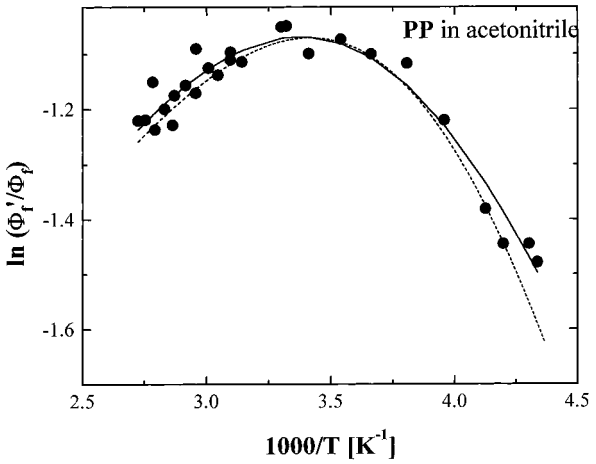

Figure 10. Stevens-Ban plot of ln[Φ_f'(ICT)/Φ_f(LE)] versus 1000/T for PP in acetonitrile. Experimental data (●). Curve (—), fit of the experimental data with eq 15, assuming that k'_f/k_f and τ'_0 do not depend on temperature. Curve (− − −), calculated (eq 15) using τ'_0 and the rate constants k_a, k_d, k_f, and k'_f obtained as a function of temperature from time-resolved measurements (Table 5). The two curves are normalized at 20 C. See text.

The dashed curve in Figure 10 is the result of a calculation (eq 15) of Φ′(ICT)/Φ(LE), employing the temperature-dependent parameters k_a, k_d, k_f'/k_f, and τ'_0 derived from the time-resolved experiments (Table 5 and Figure 8a). It shows that the incorporation of the temperature dependence of all variables appearing in eq 15 leads to a reasonable result.

Φ′(ICT)/Φ(LE) for PP and MOPP in *n*-Hexane and Acetonitrile. Role of ISC and IC. From Figure 1, it is seen that, in *n*-hexane at room temperature, the ratio Φ′(ICT)/Φ(LE) is considerably larger for MOPP than for PP, with values 3.2 and 0.11 (Table 2), respectively. In acetonitrile (Figure 2), however, similar ratios Φ′(ICT)/Φ(LE) are found: 0.34 (PP) and 0.27 (MOPP), see Table 2. This behavior can be understood by substituting the data listed in Table 5 for k_a, k_d, τ'_0, and k'_f/k_f (Figures 4c,d and 6) into eq 15.

In *n*-hexane, k_a is five times larger for MOPP than for PP, whereas ($k_d + 1/\tau'_0$), largely determined by the difference in k_d, is 11 times smaller for the former molecule (Table 5). As the ratio $k_a/(k_d + 1/\tau'_0)$ appears in eq 15, both differences lead to a nearly 50 times larger value of Φ′(ICT)/Φ(LE) for MOPP (3.1) than for PP (0.11), calculated with the ratios k'_f/k_f of 0.09 (MOPP) and 0.18 (PP). Note that these relatively small values for k'_f/k_f reduce the visibility of the ICT fluorescence in the fluorescence spectra [Φ′(ICT)/Φ(LE); eq 15] by this factor.

In acetonitrile at 20 °C, k_a is about 10 times larger for MOPP than for PP, but this difference is fully compensated by the fact that also $k_d + 1/\tau'_0$, see eq 15, is much larger (12 times) for the former molecule. With the data for k'_f/k_f (Table 5), similar values for Φ′(ICT)/Φ(LE) are then obtained for MOPP (0.27) and PP (0.35), explaining the similarity of their fluorescence spectra in acetonitrile (Figure 2).

Short ICT Lifetimes τ'_0. Rate Constants k'_{IC} and k'_{ISC}. The lifetimes τ'_o determined at 20 °C for the ICT state of PP and MOPP (Table 5) are considerably shorter, down to 28 ps for MOPP in acetonitrile, than those measured for other dual fluorescent molecules. For DMABN and a number of its derivatives in toluene, as an example, τ'_0 ranges between 2.3 and 3.1 ns.[31] To understand the reasons for this difference in τ'_0 ($1/\tau'_0 = k'_f + k'_{ISC} + k'_{IC}$), it is of interest to determine the

rate constants k'_{ISC} and k'_{IC}. This can be done by separating the overall triplet yields Φ_{ISC} (Table 1) and rate constants k_{ISC} and k_{IC} into contributions from the LE and ICT states. For this separation (eqs 16 and 17), MP was chosen as the model compound for obtaining k_{ISC} of the LE state. This choice is supported by the similarity of the values for k_{ISC}, A_{ISC}, and E_{ISC} (Table 4) of the three different phenanthridinones MP, DMPP, and TFPP in *n*-hexane as well as in acetonitrile.

$$\Phi_{ISC}(LE) = \frac{\int_0^\infty k_{ISC} c_t(LE)\, dt}{c_0(LE)} = \frac{k_{ISC}(k_d + \tau'_0{}^{-1})}{k_a \tau'_0{}^{-1} + k_d \tau_0{}^{-1} + \tau_0{}^{-1} \tau'_0{}^{-1}} \quad (16)$$

$$\Phi'_{ISC}(ICT) = \frac{\int_0^\infty k'_{ISC} c'_t(ICT)\, dt}{c_0(LE)} = \frac{k'_{ISC}\, k_a}{k_a \tau'_0{}^{-1} + k_d \tau_0{}^{-1} + \tau_0{}^{-1} \tau'_0{}^{-1}} \quad (17)$$

In eqs 16 and 17, c_0 and c_t represent the concentrations of the LE and ICT states at time zero and t, respectively. For the rate constants $k_{ISC}(LE)$ and $k'_{ISC}(ICT)$, expressions analogous to eqs 13 and 14 can be derived, using $\Phi_{ISC}(LE)$ and $\Phi'_{ISC}(ICT)$. Equations 16 and 17 are applicable to experiments with pulse excitation. They are identical to eqs 13 and 14, resulting from using the steady state approximation, as should be the case for kinetic systems containing only first-order reactions.

From the ISC rate constant k_{ISC} of the model compound MP (Table 4), $\Phi_{ISC}(LE)$ can be obtained via eq 16 by using the data for k_a, k_d, τ'_0, and τ_0 in Table 5. $\Phi'_{ISC}(ICT)$ ($=\Phi_{ISC} - \Phi_{ISC}(LE)$) can be determined from the overall triplet yields Φ_{ISC} (Table 1). The rate constant k'_{ISC} for the ICT state then follows from eq 17. The triplet yields $\Phi_{ISC}(LE)$ and $\Phi'_{ISC}(ICT)$ and the rate constants $k'_{ISC}(ICT)$ so obtained for PP and MOPP in *n*-hexane and acetonitrile at 20 °C are listed in Table 5.

For PP, $\Phi'_{ISC}(ICT)$ is considerably larger in *n*-hexane (0.43) than in acetonitrile (0.08), whereas $\Phi_{ISC}(LE)$ has similar values (0.48 and 0.40) in the two solvents. In the case of MOPP, $\Phi'_{ISC}(ICT)$ likewise decreases from *n*-hexane (0.14) to acetonitrile (0.01), whereas $\Phi_{ISC}(LE)$ is much smaller than for PP, in *n*-hexane (0.04) as well as in acetonitrile (0.02). With the onset of ICT and dual fluorescence, the importance of ISC is clearly reduced. The same picture emerges from the rate constants $k'_{ISC}(ICT)$. For PP, $k'_{ISC}(ICT)$ is much smaller in acetonitrile ($0.22 \times 10^9\ s^{-1}$) than in *n*-hexane ($3.0 \times 10^9\ s^{-1}$) at 20 °C. For MOPP, relatively small $k'_{ISC}(ICT)$ values are obtained in both solvents: $0.23 \times 10^9\ s^{-1}$ (*n*-hexane) and $0.37 \times 10^9\ s^{-1}$ (acetonitrile).

The IC rate constants $k'_{IC}(ICT)$ ($= 1/\tau'_0 - k'_f - k'_{ISC}$), obtained from τ'_0, k'_f, and k'_{ISC}, are listed in Table 5. It now follows that, with PP, ISC is the major deactivation process of the ICT state in *n*-hexane ($k'_{ISC}(ICT) = 3.0 \times 10^9\ s^{-1}$; $k'_{IC}(ICT) \cong 0.4 \times 10^9\ s^{-1}$), whereas in acetonitrile, IC has become more efficient than ISC ($k'_{ISC}(ICT) = 0.22 \times 10^9\ s^{-1}$; $k'_{IC}(ICT) = 1.4 \times 10^9\ s^{-1}$). The short ICT lifetime of PP therefore is mainly caused by ISC in *n*-hexane but by IC in acetonitrile. For MOPP, already in *n*-hexane k'_{IC} ($1.3 \times 10^9\ s^{-1}$) is larger than k'_{ISC} ($0.23 \times 10^9\ s^{-1}$), which difference strongly increases in acetonitrile: $k'_{IC} = 35 \times 10^9\ s^{-1}$ and $k'_{ISC} = 0.37 \times 10^9\ s^{-1}$, see Table 5. Note that in acetonitrile k'_{IC} is 26 times larger for MOPP than for PP. These results show that, with MOPP, IC is the dominant decay channel for the ICT state, especially in acetonitrile. From the plots in Figure 8, it is seen that for PP and MOPP in acetonitrile $k'_{ISC}(ICT)$ and also $k'_{IC}(ICT)$ do not strongly depend on temperature.

IC in ICT State of PP and MOPP via Conical Intersection. The efficient and solvent polarity dependent IC process observed here for the ICT state of PP and MOPP may be caused by the presence of a conical intersection,[36] resulting from the change in the molecular structure during the ICT reaction from the strongly twisted LE state to the planarized ICT state. With 1-(dimethylamino)naphthalene[33] and 9-cyano-10-(dimethylamino)-anthracene[32] a similar efficient and solvent polarity dependent IC process is connected with the planarization of the amino group after excitation and has likewise been attributed to the involvement of a conical intersection between the S_1 potential energy surface and the strongly displaced surface of the ground state.

Conclusion

Dual fluorescence from an LE and an ICT state is observed for the *N*-phenylphenanthridinones PP and MOPP in a number of solvents with polarities between that of *n*-hexane and acetonitrile, whereas only a single emission band is observed with DMPP and TFPP, similar to the LE fluorescence band of the model compound *N*-methylphenanthridinone (MP). The absence of dual fluorescence in the case of DMPP, in which planarization of the twisted phenyl group is hindered by the presence of two ortho-methyl substituents, indicates that such a planarization takes place during the formation of the ICT state. From solvatochromic measurements, the dipole moment of the LE state (μ_e^{LE}: 7.4 D (PP), 7.8 D (MOPP)) and the ICT state (μ_e^{ICT}: 10.6 D (PP), 13.7 D (MOPP)) states were determined. The difference between μ_e^{LE} and μ_e^{ICT} shows that the appearance of dual fluorescence is accompanied with ICT.

The fluorescence decay of DMPP, TFPP, and MP in *n*-hexane and acetonitrile is single exponential, in accord with the absence of dual fluorescence in these molecules. From the decay times and the yields of intersystem crossing and internal conversion, it is seen that ISC is the dominant decay channel of the LE state of these molecules, responsible for their relatively short decay times, between 0.24 ns for TFPP in *n*-hexane and 0.58 ns for DMPP in acetonitrile at 20 °C. The ISC activation energy E_{ISC} has values between 0.04 kcal/mol (TFPP, *n*-hexane) and 0.41 kcal/mol (DMPP, acetonitrile), which leads to the conclusion that the efficient ISC reaction is a thermoneutral $S_1(\pi\pi^*) \rightarrow T_n(n\pi^*)$ transition. Internal conversion (IC) is of minor importance for TFPP and negligible for DMPP and MP. The appearance of the ICT state opens up an efficient IC channel at the expense of ISC, with $\Phi_{IC} = 0.95$ and $\Phi_{ISC} = 0.03$ for MOPP in acetonitrile at 20 °C.

For the dual fluorescent molecules PP and MOPP, double exponential fluorescence decays are observed in *n*-hexane and acetonitrile. The amplitude ratio A_{22}/A_{21} of the ICT fluorescence response function equals −1.0, which shows that the ICT state cannot be reached by direct excitation of these molecules in the ground state, similar to what has been found with DMABN. From the activation energies E_a and E_d of the forward and backward ICT reaction of PP and MOPP in *n*-hexane, the enthalpy change ΔH for this reaction was determined: −0.9 kcal/mol (PP) and −2.4 kcal/mol (MOPP). These results are in line with the observation that the ICT rate constant k_a in *n*-hexane at 20 °C for MOPP ($108 \times 10^9\ s^{-1}$) is larger than for PP ($20 \times 10^9\ s^{-1}$). With MOPP in acetonitrile, the ICT → LE reaction could not be observed in contrast to PP, which is probably

caused by the stronger stabilization of the ICT state of MOPP as compared with that of PP ($-\Delta H = -1.5$ kcal/mol). The ICT lifetime τ'_0 of MOPP in acetonitrile at 20 °C is much shorter (0.028 ns) than in *n*-hexane (0.62 ns), because of a substantial increase in the efficiency of the IC deactivation channel (k'_{IC}) when the solvent polarity becomes larger. This increase in k'_{IC} just compensates the increase in the ICT reaction rate constant k_a, which leads to fluorescence spectra with similar Φ'(ICT)/Φ(LE) ratios for PP and MOPP in acetonitrile, see Figure 2, notwithstanding the larger ICT efficiency for the latter molecule. The internal conversion may result from a conical intersection, brought about by the change in molecular structure connected with the planarization of the twisted *N*-phenylphenanthridinones PP and MOPP during the ICT reaction.

Acknowledgment. This work was supported by the Hungarian Science Foundation (OTKA, Project No. T 33102) and by the Deutscher Akademischer Austauschdienst (DAAD, Project PPP Ungarn No 4).

Supporting Information Available: Description of the preparation and characterization (yields, melting points, MS, and NMR spectra) of MOPP, TFPP, and DMPP. This material is available free of charge via the Internet at http://pubs.acs.org.

References and Notes

(1) (a) Lippert, E.; Lüder, W.; Boos, H. In *Advances in Molecular Spectroscopy; European Conference on Molecular Spectroscopy, Bologna, Italy, 1959*; Mangini, A., Ed.; Pergamon: Oxford, U.K., 1962. (b) Lippert, E.; Lüder, W.; Moll, F.; Nägele, H.; Boos, H.; Prigge, H.; Seibold-Blankenstein, I. *Angew. Chem.* **1961**, *73*, 695.

(2) (a) Grabowski, Z. R.; Rotkiewicz, K.; Siemiarczuk, A.; Cowley, D. J.; Baumann, W. *Nouv. J. Chim.* **1979**, *3*, 443. (b) Rettig, W. *Angew. Chem., Int. Ed. Engl.* **1986**, *25*, 971. (c) Lippert, E.; Rettig, W.; Bonačič-Koutecký, V.; Heisel, F.; Miehé, J. A. *Adv. Chem. Phys.* **1987**, *68*, 1.

(3) (a) Leinhos, U.; Kühnle, W.; Zachariasse, K. A. *J. Phys. Chem.* **1991**, *95*, 5, 2013. (b) Von der Haar, Th.; Hebecker, A.; Il'ichev, Yu. V.; Jiang, Y.-B.; Kühnle, W.; Zachariasse, K. A. *Recl. Trav. Chim. Pays-Bas.* **1995**, *114*, 430. (c) Zachariasse, K. A.; Grobys, M.; Von der Haar, Th.; Hebecker, A.; Il'ichev, Yu. V.; Morawski, O.; Rückert, I.; Kühnle, W. *J. Photochem. Photobiol. A: Chem.* **1997**, *105*, 373.

(4) Rettig, W.; Bliss, B.; Dirnberger, K. *Chem. Phys. Lett.* **1999**, *305*, 8.

(5) Zachariasse, K. A. *Chem. Phys. Lett.* **2000**, *320*, 8.

(6) Demeter, A.; Druzhinin, S.; George, M.; Haselbach, E.; Roulin, J.-L.; Zachariasse, K. A. *Chem. Phys. Lett.* **2000**, *323*, 351.

(7) (a) Wintgens, V.; Valat, P.; Kossanyi, J.; Biczók, L.; Demeter, A.; Bérces, T. *J. Chem. Soc., Faraday Trans.* **1994**, *90*, 411. (b) Nemes, P.; Demeter, A.; Biczók, L.; Bérces, T.; Wintgens, V.; Valat, P.; Kossanyi, J. *J. Photochem. Photobiol. A: Chem.* **1998**, *113*, 225.

(8) (a) Valat, P.; Wintgens, V.; Kossanyi, J.; Biczók, L.; Demeter, A.; Bérces, T. *J. Am. Chem. Soc.* **1992**, *114*, 946. (b) Demeter, A.; Bérces, T.; Biczók, L.; Wintgens, V.; Valat, P.; Kossanyi, J. *J. Chem. Soc., Faraday Trans.* **1994**, *90*, 2635. (c) Wintgens, V.; Valat, P.; Kossanyi, J.; Demeter, A.; Biczók, L.; Bérces, T. *J. Photochem. Photobiol. A: Chem.* **1996**, *93*, 109. (d) Demeter, A.; Bérces, T.; Biczók, L.; Wintgens, V.; Valat, P.; Kossanyi, J. *J. Phys. Chem.* **1996**, *100*, 2001.

(9) (a) Val'kova, G. A.; Sakhno, T. V.; Shcherbo, S. N.; Shigorin, D. N.; Andrievskii, A. M.; Poplavskii, A. N.; Dyumaev, K. M. *Russian J. Phys. Chem.* **1980**, *54*, 1382. (b) Val'kova, G. A.; Sakhno, T. V.; Andrievskii, A. M. *Russian J. Phys. Chem.* **1982**, *56*, 445.

(10) (a) Lewis, F. D.; Long, T. M. *J. Phys. Chem. A* **1998**, *102*, 5327. (b) Azumaya, I.; Kagechika, H.; Fujiwara, Y.; Itoh, M.; Yamaguchi, K.; Shudo, K. *J. Am. Chem. Soc.* **1991**, *113*, 2833.

(11) (a) Zachariasse, K. A.; Grobys, M.; von der Haar, Th.; Hebecker, A.; Il'ichev, Yu. V.; Jiang, Y.-B.; Morawski, O.; Kühnle, W. *J. Photochem. Photobiol. A: Chem.* **1996**, *102*, 59. (b) Von der Haar, Th.; Hebecker, A.; Il'ichev, Yu. V.; Kühnle, W.; Zachariasse, K. A. Fast Elementary Processes in Chemical and Biological Systems, Lille, France, 1995. *AIP Conf. Proc.* **1996**, *364*, 295.

(12) Zachariasse, K. A.; Kühnle, W.; Leinhos, U.; Reynders, P.; Striker, G. *J. Phys. Chem.* **1991**, *95*, 5476.

(13) Striker, G. In *Deconvolution and Reconvolution of Analytical Signals;* Bouchy, M., Ed.; University Press: Nancy, France, 1982; p 329.

(14) Carmichael, I.; Hug, G. L. *J. Phys. Chem. Ref. Data* **1986**, *15*, 1.

(15) Demeter, A.; Bérces, T.; Zachariasse, K. A. Unpublished results.

(16) Graebe, C.; Wander, C. A. *Justus Liebigs Ann. Chem.* **1893**, *276*, 245.

(17) Srinivasan, R., Ed.; *Organic Photochemical Syntheses*; Wiley-Interscience: New York, 1971; Vol. I, p 89.

(18) Demeter, A.; Bérces, T.; Argay, G.; Kálmán, A. Unpublished results.

(19) Parusel, A.; Demeter, A.; Zachariasse, K. A. Unpublished results.

(20) Sutton, L. E. *Tables of Interatomic Distances, Spec. Publ. No. 18.*; Chemistry Society: London, 1965.

(21) Dromzee, Y.; Kossanyi, J.; Wintgens, V.; Valat, P.; Biczók, L.; Demeter, A.; Bérces, T. *Z. Kristallogr.* **1995**, *210*, 760.

(22) Baumann, W.; Bischof, H.; Fröhling, J.-C.; Brittinger, C.; Rettig, W.; Rotkiewicz, K. *J. Photochem. Photobiol. A: Chem.* **1992**, *64*, 49.

(23) Il'ichev, Yu. V.; Kühnle, W.; Zachariasse, K. A. *Chem. Phys.* **1996**, *211*, 441.

(24) Liptay, W. In *Excited States*; Lim, E. C., Ed.; Academic Press: New York, 1974; Vol. I, p 129.

(25) (a) *HyperChem*; Hypercube, Inc.: Gainesville, FL, 1994. (b) *CRC Handbook of Chemistry and Physics*, 74th ed.; Lide, D. R., Ed.; CRC Press: Boca Raton, FL, 1993.

(26) Hochstrasser, R. M.; Marzacco, C. A. In *Molecular Luminescence*; Lim, E. C., Ed.; Benjamin: New York, 1969; p 631.

(27) Lim, E. C. In *Molecular Luminescence*; Lim., E. C., Ed.; Benjamin: New York, 1969; p 469.

(28) Lim, E. C. *J. Phys. Chem.* **1986**, *90*, 6770.

(29) Birks, J. B. *Photophysics of Aromatic Molecules*; Wiley: London, 1970.

(30) Demeter, A.; Druzhinin, S.; Zachariasse, K. A. Unpublished results.

(31) Il'ichev, Yu. V.; Kühnle, W.; Zachariasse, K. A. *J. Phys. Chem. A* **1998**, *102*, 5670.

(32) Druzhinin, S.; Demeter, A.; Niebuer, M.; Tauer, E.; Zachariasse, K. A. *Res. Chem. Intermed.* **1999**, *25*, 531.

(33) (a) Rückert, I.; Demeter, A.; Morawski, O.; Kühnle, W.; Tauer, E.; Zachariasse, K. A. *J. Phys. Chem. A* **1999**, *103*, 1958. (b) Suzuki, K.; Demeter, A.; Kühnle, W.; Tauer, E.; Zachariasse, K. A.; Tobita, S.; Shizuka, H. *Phys. Chem. Chem. Phys.* **2000**, *2*, 981.

(34) Hirayama, S.; Phillips, D. *J. Photochem.* **1980**, *12*, 139.

(35) Stevens, B.; Ban, M. I. *Trans. Faraday Soc.* **1964**, *60*, 1515.

(36) Bernardi, F.; Olivucci, M.; Robb, M. A. *Chem. Soc. Rev.* **1996**, *25*, 321.